# Scanning Gate Microscopy of Quantum Contacts Opened Between Transmission Resonances

Andrii Kleshchonok, Geneviève Fleury, Jean-Louis Pichard, Gabriel Lemarié

# Scanning Gate Microscopy of Quantum Contacts Opened Between Transmission Resonances

Andrii Kleshchonok *, Geneviève Fleury, and Jean-Louis Pichard
*Service de Physique de l'État Condensé (CNRS URA 2464), IRAMIS/SPEC, CEA Saclay, 91191 Gif-sur-Yvette, France*

Gabriel Lemarié
*Laboratoire de Physique Théorique, UMR-5152, CNRS and Université de Toulouse, F 31062 France*

We study the conductance $g$ of an electron interferometer formed in a two dimensional electron gas between the charged tip of a scanning gate microscope and a nanostructured quantum contact. If the contact transmission exhibits successive resonances, we show that the images giving $g$ as a function of the tip position can exhibit novel interference rings in addition to Fabry-Pérot interference fringes spaced by half the Fermi wavelength. This is due to a beating effect between the contribution of two successive transmission peaks to $g$ and can be observed when the contact is opened between the peaks at a temperature of the order of the inter-peak energy spacing. We analytically study two contacts exhibiting the required double-peak structure: (i) The first one is made of a single quantum impurity with a parallel magnetic field, the spin degenerate Breit-Wigner resonance of its transmission being split by Zeeman effect; (ii) The second one is made of an inversion-symmetric double dot setup, where the pseudo-spin degeneracy is broken by the inter-dot coupling. Numerical studies of a quantum point contact with quantized conductance plateaus confirm that similar beating phenomena can be seen near a spin-split channel opening, when a parallel magnetic field is applied.

PACS numbers: 07.79.-v, 72.10.-d 73.63.Rt

Scanning gate microscopy (SGM) is a tool which allows to probe by electron interferometry[1] the properties of nanostructures created in a two-dimensional electron gas (2DEG). Using charged gates deposited on the surface of a semi-conductor heterostructure, one can divide the 2DEG beneath the surface in two parts connected via a more or less simple contact region. This region can be a quantum point contact[2,3] (QPC) as sketched in Fig. 1, a quantum dot[4–6], a double dot setup[7,8] or more complex nanostructures. With the charged tip of an atomic force microscope above the surface of the heterostructure, a depletion region can be capacitively induced in the 2DEG below the surface at a distance $r$ from the contact. Scanning the tip outside the contact, one can record SGM images where a color code gives the conductance $g$ of the resulting electron interferometer as a function of the tip position. These images exhibit Fabry-Pérot interference fringes spaced by half the Fermi wavelength $\lambda_F/2$, as observed by Topinka et al[9] using a QPC opened on its first conductance plateau. This has led to revisit the theory of the 2d electron interferometers[10–17] made with a QPC. These studies have shown that a very rich variety of interference phenomena can be observed if one scans a gate near a quantum contact. The interference pattern depends on the opening of the contact, on the presence of electron-electron interaction effects[12] inside the contact, and can exhibit a non trivial temperature dependence, as pointed out in Ref.[14]. At the same time, experimental SGM studies of QPCs performed at lower temperatures have revealed unexpected interference effects: (i) The interference fringes at $300mK$ exhibit[18] successive regions of enhanced and reduced contrasts as the distance $r$ between the QPC and the tip increases, with an unexplained increase of the spacing between the fringes when $r \approx 0.5\mu m$; (ii) A very recent SGM study[19] at $20mK$ shows that one can control the $0.72e^2/h$ anomaly of a QPC with a scanning gate, revealing possible relations with Wigner and Kondo physics.

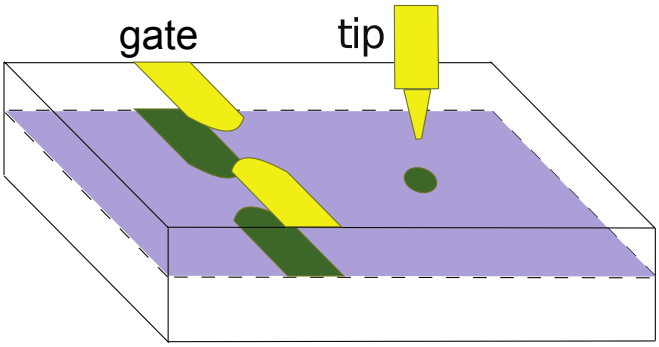


FIG. 1: (Color online) Scanning gate microscopy of a quantum contact: Metallic gates (yellow) create in the 2DEG (blue) beneath the surface a nanostuctured contact (green) which divide the 2DEG into a left and right parts. The depletion region induced by a scannable charged tip (green disk) and the contact form a 2d electron interferometer. The SGM images give the interferometer conductance as a function of the tip position.

In this paper, we discuss novel interference effects which characterize simple models where the interaction

*Present Address: Institute for Materials Science, Dresden University of Technology, Hallwachstr. 3, 01062 Dresden, Germany

effects are neglected. The role of electron-electron interaction inside the contact will be considered in a second paper, both in the perturbative and in the non perturbative (Kondo) regimes. In a previous work[14], a non interacting lattice model where the contact between two semi-infinite lattices is made of a single site (Resonant Contact Model (RCM)) was analytically solved. The transmission of such contact exhibits a single Breit-Wigner resonance. If it is opened at resonance, the contact is almost transparent for the electrons at the Fermi energy, and the interference fringes become weakly visible as the temperature $\mathcal{T} \to 0$. This is only when $\mathcal{T}$ is sufficiently large that the electrons of energy around $E_F$ start to be reflected by the contact and that the interference fringes start to be more visible. Such thermal enhancement of the interference fringes was numerically observed for a saddle point contact characterized by quantized conductance plateaus, if it is opened at the edges of the conductance plateaus. In this work, we study other thermally induced interference phenomena which can be seen if the contact transmission has at least two transmission resonances instead of a single one and if one opens it between these two resonances. A straightforward example is provided by the previously studied RCM model when the spin degeneracy of its resonance is lifted by a parallel magnetic field. We will consider the cases where the field is applied everywhere and only inside the contact. Another example is given by a lattice model where the contact is made by two sites in series instead of a single one. Such model suitable for modeling a contact made of a double-dot setup, exhibits a double peak structure of its transmission. When the two dots are identical and decoupled, there is a pseudo-spin degeneracy caused by the inversion symmetry of the model. In this second example, the inter-site hopping term in the contact plays the role of a magnetic field, and its transmission has two peaks without having to apply a magnetic field.

Using those models, we will show that interference rings can be observed in the SGM images when the contact is opened between two successive transmission resonances. These rings are not spaced by $\lambda_F/2$, but by other spacings for which we give analytical expressions. Measuring these spacings, one can determine by electron interferometry either the magnetic field in the first example, or the inter-dot coupling in the second example. The ring pattern is due to a beating effect between the contributions of transmission peaks of different spins (RCM model with field) or pseudo-spins (double-dot setup) to the SGM images. As in Ref.[14], we will eventually show that the interference mechanisms which can be analytically described for contacts exhibiting Breit-Wigner transmission peaks remain relevant for saddle-point contacts having a staircase energy dependence of their transmission with quantized number of transmission channels. This is numerically illustrated taking a QPC opened near a channel opening, when the spin degeneracy is lifted by a parallel magnetic field.

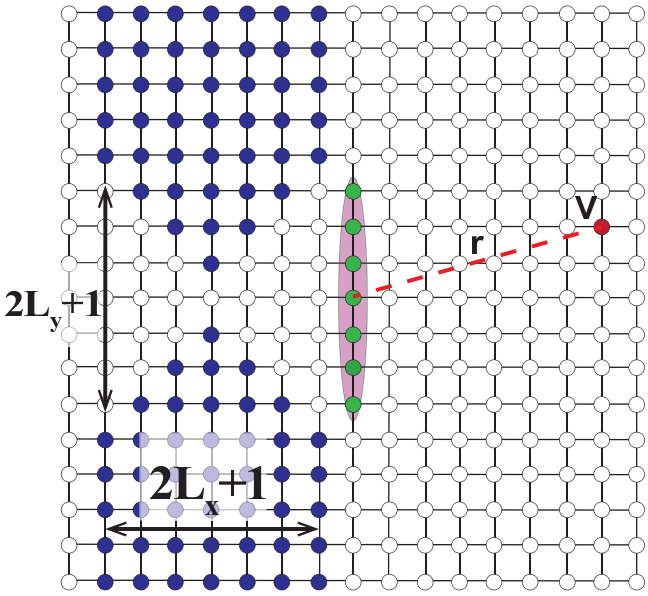


FIG. 2: (Color online) Lattice model for the SGM of a QPC: Two semi-infinite square lattices (leads) are contacted by a region of length $2L_x + 1$ and width $2L_y + 1$. In the contact region ($(-L_x \leq i_x \leq L_x)$), the potential at a site $\mathbf{i}$ of coordinates $(i_x, i_y)$ is taken infinite (blue sites) if $|i_y| \geq (L_y - k) + k\,(i_x/L_x)^2$ (Here $L_x = L_y = 3$ and $k = 2$). The depletion region induced by the charged tip is reduced to a single site of coordinates $(x, y)$ with a potential $V - 4t$. Without tip ($V = 0$), the QPC transmission $T_0(E)$ is given by a staircase function, each channel opening giving rise to a new step.

## I. LATTICE MODELS FOR QUANTUM CONTACTS

For studying the 2D interferometer formed in a 2DEG between a QPC and the depletion region induced by a scanning gate microscope, we will use lattice models where two semi-infinite square lattices (leads) are connected by a small contact region of length $2L_x + 1$ and maximum width $2L_y + 1$. $c_{\mathbf{i}\sigma}$ ($c^\dagger_{\mathbf{i}\sigma}$) being the destruction (creation) operator of an electron of spin $\sigma$ at site $\mathbf{i}$ of coordinates $(i_x, i_y)$, and $n_{\mathbf{i}\sigma} = c^\dagger_{\mathbf{i}\sigma} c_{\mathbf{i}\sigma}$, the Hamiltonians of the left ($i_x \leq -L_x$) and right ($i_x \geq L_x$) leads read

$$H_{leads} = \sum_{\mathbf{i},\sigma} \left( -4t n_{\mathbf{i}\sigma} + t \sum_{\mathbf{j}} c^\dagger_{\mathbf{i}\sigma} c_{\mathbf{j}\sigma} \right) + H.C. \qquad (1)$$

The hopping terms are non-zero between nearest neighbors sites $\mathbf{i}, \mathbf{j}$ only. The energy scale is defined by taking $t = -1$, such that the conduction bands of the leads are in the energy interval $[0, 8]$ when the site potentials are equal to $-4t$. Hereafter, we will study the continuum limit ($E \ll 1$). The Hamiltonian of the contact reads

$$H_{contact} = \sum_{\mathbf{i},\sigma} \left( (V_{\mathbf{i}} - 4t) n_{\mathbf{i}\sigma} + t \sum_{\mathbf{j}} c^\dagger_{\mathbf{i}\sigma} c_{\mathbf{j}\sigma} \right) + H.C. \quad (2)$$

The summations are restricted to $-L_x \leq i_x \leq L_x$ and to $-L_y \geq i_y \leq L_y$. Moreover, the site potentials $V_{\mathbf{i}}$ are taken infinite inside the contact region if $|i_y| \geq (L_y - k) + k\,(i_x/L_x)^2$, where $k$ is a parameter. This restricts the electron motion inside a smoothly opening region known to favor a sharp opening of the conductance channels as one increases the energy. A smooth opening reduces also the interference effects induced by the back-scattering of electron waves leaving the contact region, effects which induce oscillations in the transmission function $T(E)$. The Hamiltonians describing the coupling between the contact and the two leads read

$$H_c^l = t_c \sum_{i_y=-L_y,\sigma}^{L_y} \left( c^\dagger_{(-L_x,i_y)\sigma} c_{(-L_x-1,i_y)\sigma} + H.C. \right), \quad (3)$$

$$H_c^r = t_c \sum_{i_y=-L_y,\sigma}^{L_y} \left( c^\dagger_{(L_x,i_y)\sigma} c_{(L_x+1,i_y)\sigma} + H.C. \right). \quad (4)$$

In this simplified model, the QPC Hamiltonian reads $H_0 = H_{contact} + \sum_{j=l,r}(H_c^j + H_{leads}^j)$. The QPC transmission $T_0(E)$ is a staircase function, each stair taking an integer value which counts the number of open channels. To describe the depletion region induced by the charged tip, a term $H_{tip}(x,y) = \sum_\sigma V n_{\mathbf{T}\sigma}$ is added to $H_0$, which modifies by an amount $V$ the potential $-4t$ of a single site $\mathbf{T}$ of coordinates $(x,y)$ located at a distance $r = \sqrt{x^2+y^2}$ from the contact. The interferometer Hamiltonian reads $H = H_0 + H_{tip}(x,y)$. Fig. 2 shows such an interferometer when $L_x = L_y = 3$ and $k = 2$.

Before studying the SGM of a QPC when $L_x$ and $L_y$ are large, it is very instructive to study the limit shown in Fig. 3 where the contact is reduced to a single site $\mathbf{I}$ of coordinates $(0,0)$ and potential $-4t+V_{\mathbf{I}}$. This defines the resonant contact model (RCM) which can be solved analytically[14] when the width of the leads becomes infinite. As one varies the energy $E$ for $t_c \ll 1$ and $V = 0$, the RCM transmission function $T_0(E)$ exhibits a single spin-degenerate Breit-Wigner resonance, and not the usual staircase function which characterizes the QPC conductance quantization.

## II. SGM OF THE RESONANT CONTACT MODEL

### A. RCM model: Spin-degenerate case at $\mathcal{T} = 0$

Let us first study analytically the SGM of the RCM model where the contact is made with a single site ($L_x = L_y = 0$). Without tip, the transmission of an electron of spin $\sigma$ and energy $E$ through the RCM contact is given by the Fisher-Lee formula[20]:

$$T_0^\sigma(E) = \mathrm{Tr}\left[\Gamma_l(E) G_0^R(E) \Gamma_r(E) G_0^A(E)\right], \quad (5)$$

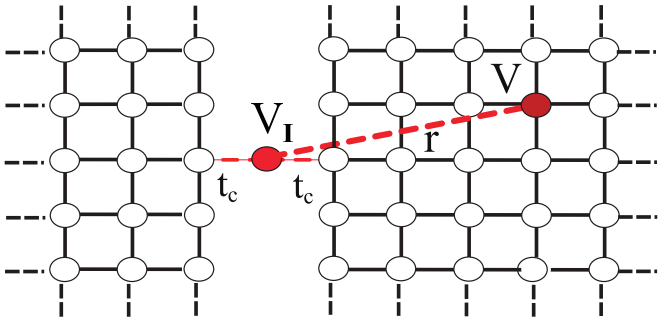


FIG. 3: (Color online) SGM of the Resonant Contact Model (RCM): Two semi-infinite square lattices are contacted via a single site $\mathbf{I}$ of coordinates $(0,0)$, potential $V_{\mathbf{I}}$ and coupling term $t_c$. Adding a potential $V$ at a site $\mathbf{T}$ of coordinates $(x,y)$ gives rise to an electron interferometer of size $r = \sqrt{x^2+y^2}$.

where $G_0^R$ is the retarded Green's function of the contact dressed by the right (r) and left (l) leads:

$$G_0^R(E) = \lim_{\eta \to 0^+} (E + i\eta - 4 - V_{\mathbf{I}} - \Sigma_l^R - \Sigma_r^R)^{-1}. \quad (6)$$

The contact being reduced to a single site $\mathbf{I}$ coupled to another single site per lead, the lead self-energies $\Sigma_{l,r}(E)$ are only two complex numbers $\Sigma_{l,r}(E) = R_{l,r}(E) + iI_{l,r}(E) = t_c^2 < \pm 1, 0 | G_{l,r}^R(E) | \pm 1, 0 >$, $G_{l,r}^R(E)$ being the retarded Green's function of the left and right leads evaluated at the sites directly coupled to $\mathbf{I}$. The coupling rates to the right and left leads verify: $\Gamma_{r,l} = i(\Sigma_{r,l}^R - \Sigma_{r,l}^A)$. Using the method of mirror images[21], $G_{l,r}^R(E)$ can be expressed in terms of the Green's function $G_{2d}^R(E)$ of the infinite 2d square lattice[22]. Without tip ($V = 0$), one gets:

$$T_0^\sigma(E) = \frac{4 I_r I_l}{(E - 4 - V_{\mathbf{I}} - R_r - R_l)^2 + (I_r + I_l)^2}. \quad (7)$$

If the variation of $\Sigma_{l,r}(E)$ can be neglected when $E$ varies inside the resonance (typically $t_c < 0.5$ in the continuum limit where the Fermi momentum $k_F \ll 1$), this is a Lorentzian of width $\Gamma = -2I$ and center $4 + V_{\mathbf{I}} + 2R$ since $R_l = R_r \equiv R$ and $I_r = I_l \equiv I$.

If one adds a tip potential $V \neq 0$ in the right lead, the effect of the tip can be included by adding an amount $\Delta\Sigma_r(E) = \Delta R_r(E) + i\Delta I_r(E)$ to $\Sigma_r(E)$ (see Refs.[14,23]). The interferometer transmission $T^\sigma(E)$ is still given by Eq. (7), once $R_r + \Delta R_r$ and $I_r + \Delta I_r$ have been substituted for $R_r$ and $I_r$. The effect of the tip being restricted to a single site $\mathbf{T}$, $\Delta\Sigma_r$ can be obtained from Dyson's equation for $G_{r+V}(E)$ the Green's function of the right lead with the tip potential:

$$< 1,0|G_{r+V}^R(E)|1,0 > = < 1,0|G_r^R(E)|1,0 > + \frac{< 1,0|G_r^R(E)|\mathbf{T} > V < \mathbf{T}|G_r^R(E)|1,0 >}{1 - V < \mathbf{T}|G_r^R(E)|\mathbf{T} >} \quad (8)$$

In the continuum limit and for distances $r \gg k_F^{-1}$, one

finds:

$$\frac{\Delta\Sigma_r}{t_c^2\rho} \approx -\frac{k_F x^2}{2\pi r^3}\exp[i(2k_F r+\pi/2+\phi)] + O(\frac{x^{3/2}}{r^3}), \quad (9)$$

where $\rho$ and $\phi$ are the modulus and the phase of the amplitude of diffusion of the tip potential $V/(1 - V\langle 0,0|G^R_{2d}(E)|0,0\rangle)$. In the continuum limit, one can also approximate $I \approx -t_c^2 k_F^2/4$. Therefore, at sufficiently large distances $r \gg \lambda_F/2$, $\Delta\Sigma_r^R(E) \ll I$ and one can expand $T^\sigma(E)$ to the leading order $\propto x^2/r^3$ in $\Delta\Sigma_r$:

$$\frac{T^\sigma(E)-T_0^\sigma(E)}{T_0^\sigma(E)} \approx -s\sqrt{T_0^\sigma(E)(1-T_0^\sigma(E))}\,\frac{\Delta R_r(E)}{I} + (1-T_0^\sigma(E))\,\frac{\Delta I_r(E)}{I}, \quad (10)$$

where $s = \mathrm{sign}[V_{\mathbf{I}}^{res} - V_{\mathbf{I}}]$ and $V_{\mathbf{I}}^{res} \equiv E - 4 - 2R$ is the value of $V_{\mathbf{I}}$ where $T_0^\uparrow = T_0^\downarrow = 1$. This leads to the simple prediction:

$$\frac{T^\sigma(E)-T_0^\sigma(E)}{T_0^\sigma(E)} \approx A_0\cos(2k_F r+\Phi_0) + O\left(\frac{x^{3/2}}{r^3}\right) \quad (11)$$

where the amplitude $A_0 = \frac{2\rho}{\pi k_F}\frac{x^2}{r^3}\sin\zeta_0$ decreases as $\frac{x^2}{r^3}$, the phase $\Phi_0 = \pi/2+\phi-\zeta_0$ and $\sin\zeta_0 = -s\sqrt{1-T_0^\sigma(E)}$. Eq. (11) describes the Fabry-Pérot fringes spaced by $\lambda_F/2$ and their decay with $r$, assuming $T_0^\sigma(E) < 1$. One needs to take into account corrections of higher order[14] when $T_0^\sigma(E) \approx 1$, a limit which we will not consider in this work.

### B. RCM model: Spin-degenerate case at $\mathcal{T} \neq 0$

Let us now study the effect of the tip upon the conductance in units of $e^2/h$ at a temperature $\mathcal{T}$:

$$\Delta g = g - g_0 = \sum_\sigma \int dE(T^\sigma(E) - T_0^\sigma(E))(-\frac{\partial f}{\partial E}), \quad (12)$$

where $f$ is the Fermi-Dirac distribution. We shall consider in the following the case of a sharp Lorentzian resonance ($t_c < 0.5$) of the transmission $T_0^\sigma(E)$. Then, $R$ and $I$ do not vary rapidly inside the resonance. In the same way, the amplitude of diffusion of the tip, characterized by $\rho$ and $\phi$, vary slowly inside the resonance and thus can be considered as constants. In order to calculate the integral (12) analytically, we make the approximation[10] $-\partial f/\partial E \approx (1/4k_B\mathcal{T})\exp -[\sqrt{\pi}(E - E_F)/(4k_B\mathcal{T})]^2$, where $E_F$ and $k_B$ are the Fermi energy and the Boltzmann constant. Then, we obtain that $\Delta g = D_1 + D_2$ where:

$$D_1 \approx \frac{2\rho}{\pi^{3/2}k_F}\frac{x^2}{r^3}\frac{l_\mathcal{T}}{l_\Gamma}\,\Re\left[e^{i(2k_F r+\phi+\pi/2)}\int_{-\infty}^{\infty}\frac{q+v}{[1+(q+v)^2]^2}e^{-\left(\frac{l_\mathcal{T}}{l_\Gamma}q\right)^2}e^{i\frac{r}{l_\Gamma}q}\,\mathrm{d}q\right], \quad (13)$$

$$D_2 \approx \frac{2\rho_T}{\pi^{3/2}k_F}\frac{x^2}{r^3}\frac{l_\mathcal{T}}{l_\Gamma}\,\Im\left[e^{i(2k_F r+\phi_T+\pi/2)}\int_{-\infty}^{\infty}\frac{(q+v)^2}{[1+(q+v)^2]^2}e^{-\left(\frac{l_\mathcal{T}}{l_\Gamma}q\right)^2}e^{i\frac{r}{l_\Gamma}q}\,\mathrm{d}q\right]. \quad (14)$$

$v \equiv (V_{\mathbf{I}}^{res} - V_{\mathbf{I}})/\Gamma$ gives the energy shift of $V_{\mathbf{I}}$ from the resonance $V_{\mathbf{I}}^{res}$ in units of $\Gamma$, and $q = (E-E_F)/\Gamma$. $l_\mathcal{T}$ and $l_\Gamma$ are the two length scales associated respectively to $\mathcal{T}$ (Fermi-Dirac statistics) and to $\Gamma$ (resonant transmission):

$$l_\mathcal{T} = \frac{\sqrt{\pi}k_F}{4k_B\mathcal{T}} \quad (15)$$

$$l_\Gamma = \frac{k_F}{\Gamma}. \quad (16)$$

Calculating the Fourier transforms $D_1$ and $D_2$, we eventually obtain the following results:

$$\Delta g(\mathcal{T}) \approx 2A(\mathcal{T})\cos(2k_F r+\Phi(\mathcal{T})), \quad (17)$$

where in the large distance regime $r > r^* \equiv 2l_\mathcal{T}[1 + l_\mathcal{T}(1+|v|)/l_\Gamma]$:

$$A(\mathcal{T}) = \frac{\rho x^2 l_\mathcal{T}}{\sqrt{\pi}k_F r^3}\exp -[(1+v^2)(\frac{l_\mathcal{T}}{l_\Gamma})^2 + \frac{r}{l_\Gamma}] \quad (18)$$

$$\Phi(\mathcal{T}) = \phi + v\frac{r}{l_\Gamma} - 2v(\frac{l_\mathcal{T}}{l_\Gamma})^2. \quad (19)$$

The factor 2 in $\Delta g(\mathcal{T})$ comes from the spin degeneracy. In Fig. 4, one can see that the above expressions reproduce accurately the numerical results without adjustable parameters.

### C. RCM model: Effect of a parallel magnetic field

Let us consider now the case where a uniform parallel magnetic field is applied upon the 2DEG. The spin degeneracy is broken and the electrons of opposite spin have energies which are shifted ($E^\sigma \to E(h=0) \pm h$) and which contribute to transport with different wavevectors. When $E_F$ is small enough, we can use the continuum dispersion relation $k^\sigma = \sqrt{E^\sigma}$. If the Zeeman energy $h$ remains small compared to $E_F$, the 2DEG is not fully polarized. In Fig. 5, the conductance $g_0$ of the

RCM contact is given as a function of the contact potential $V_I$. One can see how the spin degenerate peak of conductance ($h = 0$) of width $\Gamma$ is split by the field ($h = 8\Gamma$) for increasing values of $\mathcal{T}$. Hereafter, we study the SGM image at the symmetric point indicated by an arrow, where $V_{\mathbf{I}} = V_{\mathbf{I}}^{res}(h = 0)$.

The relative effect of the tip upon the transmission of an electron of spin $\sigma$ at an energy $E$ becomes,

$$\frac{T^\sigma(E) - T_0^\sigma(E)}{T_0^\sigma(E)} \approx A_0^\sigma \cos(2k_F^\sigma r + \Phi_0^\sigma) + O\left(\frac{x^{3/2}}{r^3}\right) \quad (20)$$

where $A_0^\sigma = (2\rho^\sigma)/(\pi k_F^\sigma)(x^2/r^3)\sin\zeta_0^\sigma$, $\Phi_0^\sigma = \pi/2 + \phi^\sigma - \zeta_0^\sigma$, $\sin\zeta_0^\sigma = -s^\sigma\sqrt{1 - T_0^\sigma(E)}$ and $s^\sigma = \mathrm{sign}(V_I^{res} - V_I)$. If the contact is opened in the middle between the two transmission peaks, $s^\uparrow = -s^\downarrow$, $\sin\zeta_0^\uparrow = -\sin\zeta_0^\downarrow$. The contribution of electrons of opposite spins to $\sum_\sigma (T^\sigma(E) - T_0^\sigma(E))/T_0^\sigma(E)$ have opposite signs when the tip is put at a distance

$$r^{\mathcal{D}} = \frac{2\pi n + (\phi^\downarrow - \phi^\uparrow) + (\rho^\uparrow - \rho^\downarrow)}{2(k_F^\uparrow - k_F^\downarrow)} , \quad (21)$$

where $n$ is integer $(0, 1, 2, \ldots)$. At a temperature $\mathcal{T} = 0$, this means that the SGM image of a contact opened between its two transmission resonances exhibits a pattern of rings of radii $r^{\mathcal{D}}$, where the beating between the contribution of opposite spin is destructive. In contrast, the beating becomes constructive on rings of radii $r^{\mathcal{C}}$. If we neglect the spin dependence of the transmission without tip at the symmetric point, ($T_0^\sigma \approx T_0$)) these radii are given by

$$r^{\mathcal{D}}(n) \approx \frac{\pi n + \arcsin(\sqrt{1 - T_0})}{\sqrt{E_F + h} - \sqrt{E_F - h}} \quad (22)$$

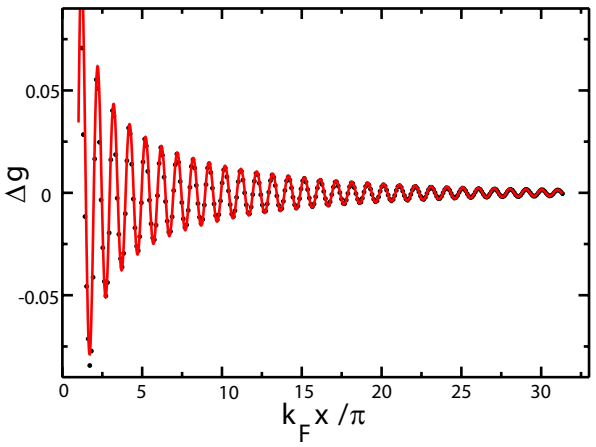


FIG. 4: (color online) SGM of the RCM model at a temperature $\mathcal{T} = 0.5\Gamma$: Numerical calculations (black points) of $\Delta g(x, y = 0)$ as a function of $k_F x/\pi$. The numerical results coincide with the analytical results (red line - Eq. (17)) without adjustable parameters. $l_{\mathcal{T}} = 7\lambda_F/2$ and $l_\Gamma = 16\lambda_F/2$ for $E_F = 0.1$, $V = -2$ (i.e. $\rho \approx 3.91$, $\phi \approx -1.71$, $k_F \approx 0.317$), $t_c = 0.2$ and $v = 0.5$).

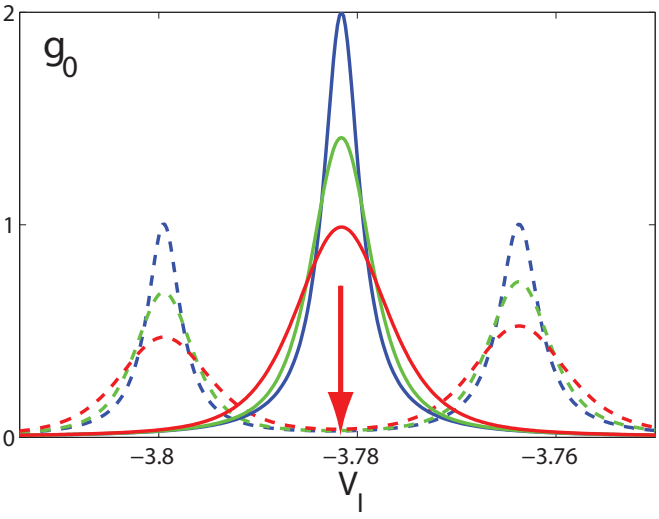


FIG. 5: (Color online) RCM Conductance $g_0$ (in units of $e^2/h$) without field ($h = 0$, solid line) and with field ($h = 8\Gamma$, dashed line) as a function of $V_{\mathbf{I}}$ for $\mathcal{T} = 0$ (blue) $\mathcal{T} = \Gamma/2$ (green) and $\mathcal{T} = \Gamma$ (red). There is no tip ($V = 0$) and $\Gamma = 0.003$ ($t_c = 0.2$ and $E_F = 0.15$). The parallel magnetic field is applied everywhere and a small asymmetry can be seen between the right and left peaks. The arrow gives the symmetric point where the SGM images are studied.

$$r^{\mathcal{C}}(n) \approx \frac{(n + 1/2)\pi + \arcsin(\sqrt{1 - T_0})}{\sqrt{E_F + h} - \sqrt{E_F - h}} . \quad (23)$$

In Fig. 6, one can see how looks an SGM image taken with a parallel magnetic field at $\mathcal{T} = 0$: The Fabry-Perot fringes spaced by $\lambda_F/2$ are modulated by the beating effect between the contribution of opposite spins. We can see the three first rings at the expected radii $r^{\mathcal{D}}(n)$ with $n = 0, 1, 2$, where the effect of the tip upon the interferometer conductance disappears, separated by regions centered around rings of radii $r^{\mathcal{C}}(n)$ where the visibility of the fringes is enhanced by the applied magnetic field.

When the temperature $\mathcal{T} \neq 0$ but satisfies the condition $\mathcal{T}/\Gamma \ll v$, the expressions can be simplified if $r \ll 2l_{\mathcal{T}}\left[1 + (l_{\mathcal{T}}/l_\Gamma)(1 + |v|)\right]$. One finds that the SGM images are roughly identical to those described by Eq. (20) for $\mathcal{T} = 0$ within a circle of radius $l_{\mathcal{T}}$, and suppressed outside (see Fig. 7).

$$\Delta g(\mathcal{T}, h) \approx \Delta g(\mathcal{T} = 0, h) \exp -(\frac{r}{2l_{\mathcal{T}}})^2 . \quad (24)$$

At higher temperatures ($\mathcal{T}/\Gamma \geq v$) and larger distances $r \gg 2l_{\mathcal{T}}\left[1 + (l_{\mathcal{T}}/l_\Gamma)(1 + |v|)\right]$, $\Delta g(\mathcal{T})$ is given by $\sum_\sigma A^\sigma(\mathcal{T})\cos(2k_F^\sigma r + \Phi^\sigma(\mathcal{T}))$ where $A^\sigma(\mathcal{T})$ and $\Phi^\sigma(\mathcal{T})$ are defined in Eq. (18) and Eq. (19) with $\sigma$-dependent variables. One finds that the interference fringes of each spin orientation cancel on rings of radii

$$r^{\mathcal{D}}(n) = \frac{\pi(1 + 2n) + 2\left[\Delta\tilde{v} - \Delta\phi\right]}{2\Delta k_F + \Delta w} , \quad (25)$$

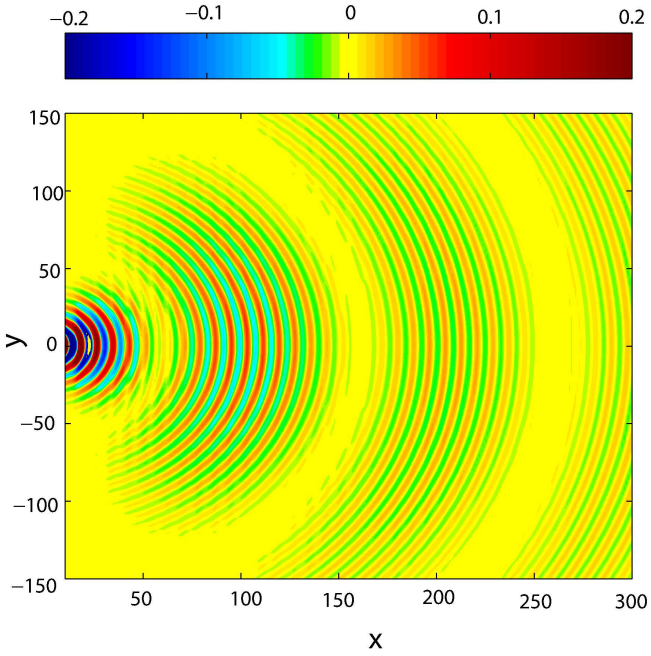


FIG. 6: (Color online) Zero temperature and parallel magnetic field applied everywhere: Relative effect (upper color scale) of the tip ($V = -2$) upon the RCM transmission $\Delta T/T_0$ as a function of tip coordinates $(x, y)$. Zeeman energy $h = 4\Gamma \approx 0.0119$, $t_c = 0.2$ and $E_F = 0.15$. The contact potential has the value $V_I$ indicated by the arrow in Fig. 5 (symmetric point) where $T_0 = 0.12$ and $\Gamma \approx 0.003$.

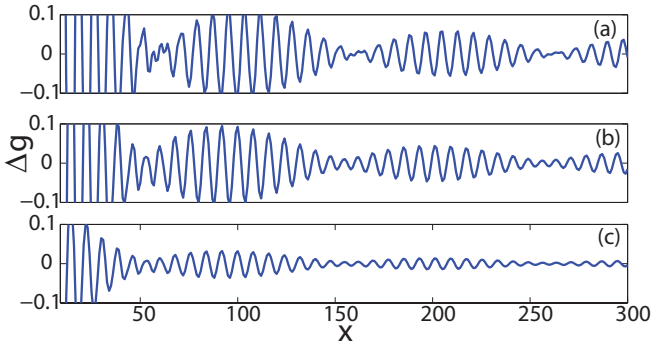


FIG. 7: (Color online) RCM contact in the presence of a parallel magnetic field $h = 4\Gamma \approx 0.0119$ applied everywhere: $\Delta g$ as a function of the tip coordinates $(x, y = 0)$ with $E_F = 0.15$, $V = -2$, $t_c = 0.2$ and $\Gamma \approx 0.003$. The figures (a) $\mathcal{T} = 0$, (b) $\mathcal{T} = 10^{-4}$, (c) $\mathcal{T} = 8 \times 10^{-4}$ are in the regime $\mathcal{T}/\Gamma \ll v$. The location $r^{\mathcal{D}}(n)$ of the destructive interferences is independent of the temperature $\mathcal{T}$, in agreement with Eq. (24).

where $\Delta\tilde{v} = \left[v(l_{\mathcal{T}}/l_\Gamma)^2\right]^\uparrow - \left[v(l_{\mathcal{T}}/l_\Gamma)^2\right]^\downarrow$, $\Delta\phi = \phi^\uparrow - \phi^\downarrow$, $\Delta k_F = k_F^\uparrow - k_F^\downarrow$ and $\Delta w = [v/l_\Gamma]^\uparrow - [v/l_\Gamma]^\downarrow$. $n = 0, 1, 2, \ldots$ is an integer.

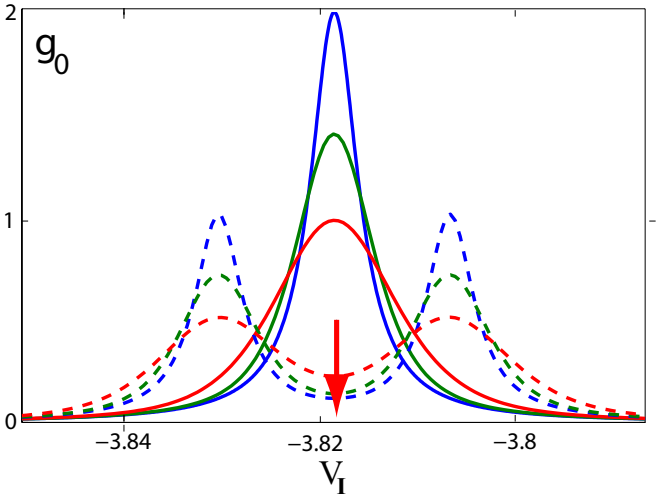


FIG. 8: (Color online) RCM contact with a magnetic field restricted to the contact. Conductance $g_0$ (in units of $e^2/h$) without tip ($V = 0$, $t_c = 0.2$, and $\Gamma = 0.003$) as a function of $V_{\mathbf{I}}$ for $\mathcal{T} = 0$ (blue) $\mathcal{T} = \Gamma/2$ (green) and $\mathcal{T} = \Gamma$ (red). The Zeeman term shifts only the potential of the contact $V_{\mathbf{I}} \to V_{\mathbf{I}} \pm h$: Cases with ($h = 0$, solid line) and without spin degeneracy ($h = 4\Gamma$, dashed line). The arrow gives the potential $V_{\mathbf{I}}$ where the effect of the tip will be studied (symmetric point).

### D. RCM model: Effect of a parallel magnetic field restricted to the contact

Let us consider now the case where a local parallel magnetic field is not applied upon the leads, but only upon the contact. This removes the spin degeneracy in the contact by a local Zeeman term $\pm h$. This implies to shield the applied field outside the contact. An alternative way of having a local Zeeman term would consist in taking an Anderson impurity for the contact (the RCM model plus a local Hubbard interaction $U n_I^\uparrow n_I^\downarrow$ in the contact). In that case, a spontaneous magnetic moment would be created in the contact if $U > \Gamma$ for temperatures in the range $\mathcal{T}_K < \mathcal{T} < \sqrt{U\Gamma}$, $\mathcal{T}_K$ being the Kondo temperature. Such a case without an external applied field will be discussed in a following paper. Here, we consider the simpler case where a local Zeeman term is induced by an applied field. Its effect upon the conductance $g_0$ of the contact is illustrated in Fig. 8, $g_0^\uparrow(\mathcal{T})$ having a peak shifted by an amount $v^\uparrow = -h/\Gamma$ (electron with parallel spin) while the shift is $v^\downarrow = h/\Gamma$ for the antiparallel spin. In contrast to the case where the field is applied everywhere, $k_F$ and hence $l_{\mathcal{T}}$ and $l_\Gamma$ do not depend on $\sigma$, while $\Delta\phi = 0$. Moreover one has $v_\uparrow = -v_\downarrow$ at the symmetric point indicated by an arrow in fig. 8. This allows us to simplify Eq. (25) and to obtain

$$r^{\mathcal{D}}(n) = \frac{2k_F}{\Gamma}\left(\frac{l_{\mathcal{T}}}{l_\Gamma}\right)^2 + \left(n + \frac{1}{2}\right)\frac{\pi k_F}{h}, \qquad (26)$$

$(n = 0, 1, \ldots)$ for the radii of the rings where the effect of the tip is suppressed by the magnetic field. Conversely,

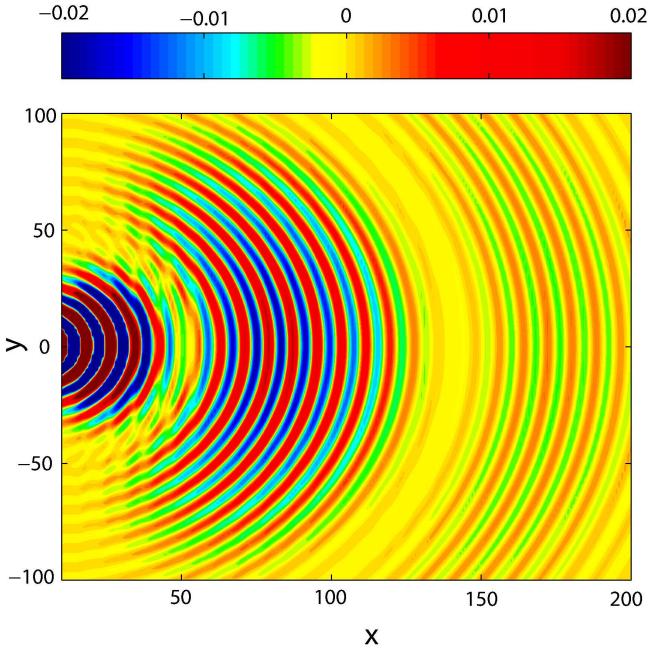


FIG. 9: (Color online) RCM contact with a Zeeman term $h = \pm 0.0136$ in the contact. $E_F = 0.15$ and $\lambda_F/2 = 8.1$. $\Delta g/g_0(\mathcal{T}^*, \Gamma^*)$ as a function of the coordinates $(x, y)$ of the tip (potential $V = -2$). $\mathcal{T}^* = 0.0099$, $\Gamma^* = 0.0035$. The parameters have been chosen such that the radius (Eq. (26)) of the first ring $r^{\mathcal{D}}(n = 0) = 50$.

the oscillations of $\Delta g^{\uparrow}(\mathcal{T})$ and $\Delta g^{\downarrow}(\mathcal{T})$ add if the distance $r$ is given by $r^{\mathcal{C}}(n) = r^{\mathcal{D}}(n) + \pi k_F/(2h)$. The SGM image giving $\Delta g(\mathcal{T})$ as a function of the tip position is characterized by a first ring at a distance $r^{\mathcal{D}}(n = 0)$ followed by other rings spaced by $\pi k_F/h$ where $\Delta g(\mathcal{T}) = 0$. To optimize the contrast in the images, we calculate for a given value of $h$ the temperature $\mathcal{T}^*$ and the width $\Gamma^*$ for which $\Delta g(\mathcal{T}, r = r^{\mathcal{C}}(n = 0))$ is maximum. The extrema are given by the conditions $\partial A/\partial l_\Gamma = 0$ and $\partial A/\partial l_{\mathcal{T}} = 0$. One obtains two coupled non-linear algebraic equations which can be solved numerically, yielding $\mathcal{T}^* \approx 0.73h$ and $\Gamma^* \approx 0.25h$. Let us note that the observation of the rings in the pattern of Fabry-Pérot fringes is only possible if their spacing exceeds $\lambda_F$, i. e. if $h < (\pi/\lambda_F)^2$. In Fig. 9, one can see an SGM image exhibiting the ring pattern induced by a local Zeeman term $h$ when $\mathcal{T} = \mathcal{T}^*$ and $\Gamma = \Gamma^*$. Eventually, we show in Fig. 10 how the radii of the rings where the effect of the tip is suppressed by a local field depend on $\mathcal{T}$ and $h$. For a fixed value of $\Gamma$, one can see how $r^{\mathcal{D}}(n) \to \infty$ when $\mathcal{T} \to 0$ or $h \to 0$, making impossible to observe the pattern of rings in the SGM image.

In Fig. 11, $\Delta g(x, y = 0)/g_0$ is shown as one varies the coordinate x of the tip in the presence of a field acting on the contact. One can see the pattern of interferences characterizing three different values of $h$, when the temperature $\mathcal{T}$ and the resonance width $\Gamma$ take their optimal values $\mathcal{T}^*$ and $\Gamma^*$.

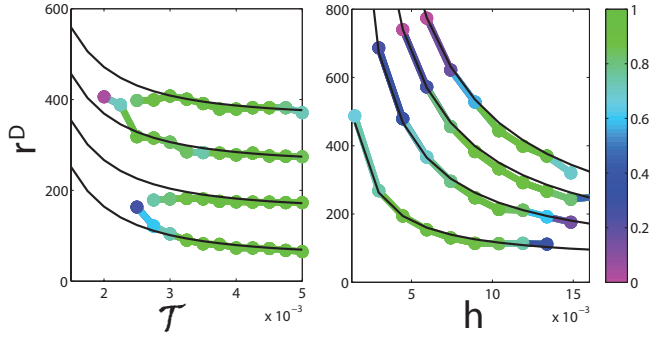


FIG. 10: (Color online) RCM contact with local field and $\Gamma = 0.003$: Radii $r^{\mathcal{D}}(n)$ of the rings for $n = 0, 1, 2$ and 3 as a function of $\mathcal{T}$ (left, $h = 0.01$) and of the local Zeeman term $h$ (right, $\mathcal{T} = 0.0028$). The dots are obtained numerically, their colors corresponding to a visibility scale indicated at the right (0 without contrast, 1 for the best contrast). The solid lines give the analytical expression (26) for $r^{\mathcal{D}}(n)$ which was derived assuming $r^{\mathcal{D}}(n) > r^*$.

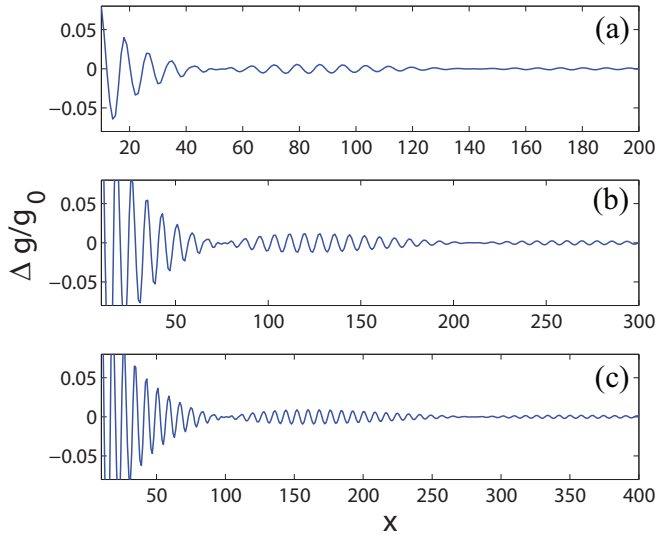


FIG. 11: (Color online) RCM contact with a Zeeman term $h$ in the contact: $\Delta g/g_0(\mathcal{T}^*, \Gamma^*, y = 0)$ is plotted as a function of $x$ for a tip potential $V = -2$. $E_F = 0.1542$ and $\lambda_F/2 = 8$. (a): $h = 0.0136$, $\mathcal{T}^* = 0.0099$, $\Gamma^* = 0.0035$ (b): $h = 0.0091$, $\mathcal{T}^* = 0.0066$, $\Gamma^* = 0.0023$; (c): $h = 0.0068$, $\mathcal{T}^* = 0.005$, $\Gamma^* = 0.0017$.

Let us underline the difference between the effect of a field restricted to the contact or applied everywhere. In the first case (see Eq. (26)), the first ring has a radius $r^{\mathcal{D}}(n = 0) \to \infty$ as $\mathcal{T} \to 0$: The first destructive interference cannot be seen. It is only when one increases $\mathcal{T} \to \mathcal{T}^*$ that $r^{\mathcal{D}}(n = 0)$ becomes small enough and that the destructive interference caused by a local field can be seen. In the second case, Eq. (24)) implies that the pattern of rings does not depend on the temperature when $r \ll l_{\mathcal{T}}$ and can be seen even when $\mathcal{T} \to 0$. Illustrations of the differences of the SGM images when a field is ei-

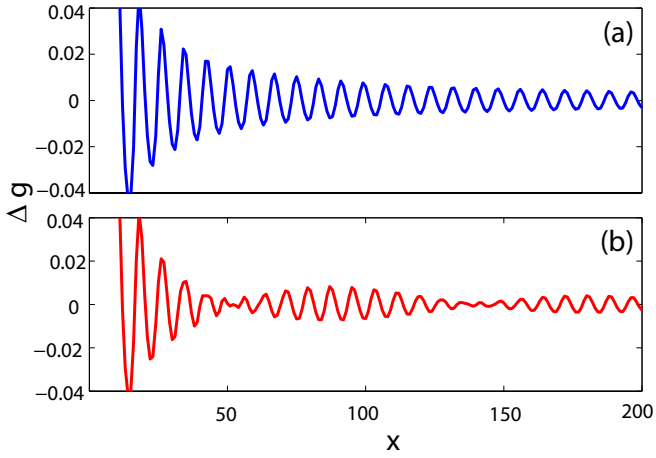


FIG. 12: (Color online) RCM contact with parallel magnetic field $h = 0.0136$, $E_F = 0.1542$, $\Gamma^* = 0.0035$ and $\lambda_F/2 = 8$: For a temperature $\mathcal{T} = 0$, $\Delta g(x, y = 0)$ is plotted as a function of $x$ for a tip potential $V = -2$. Fig. (a): The field is applied only inside the contact and no beating effect can be observed, since $r^D(n = 0) \to \infty$ when $\mathcal{T} \to 0$. Fig. (b): The same field is applied everywhere and the beating effect is very visible when $\mathcal{T} \to 0$.

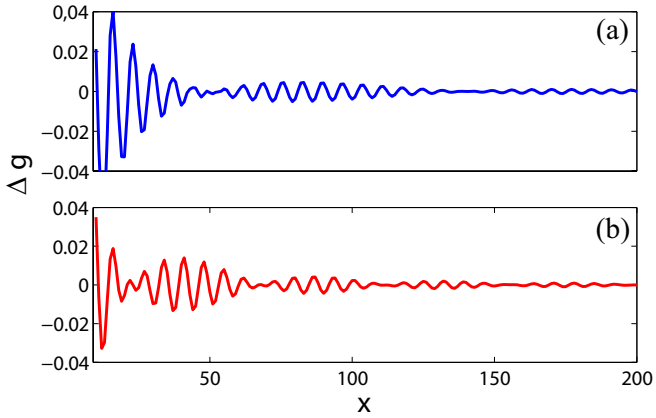


FIG. 13: (Color online) RCM contact with parallel magnetic field $h = 0.0136$, $E_F = 0.1542$, $\Gamma^* = 0.0035$ and $\lambda_F/2 = 8$: For a temperature $\mathcal{T}^* = 0.0099$, $\Delta g(x, y = 0)$ is plotted as a function of $x$ for a tip potential $V = -2$. (a): Magnetic field inside the contact only ($k_F^\uparrow = k_F^\downarrow$). (b): Magnetic field everywhere ($k_F^\uparrow \neq k_F^\downarrow$). The difference of periodicity and frequency are mainly due to the field dependence of $k_F^\sigma$.

ther applied everywhere or restricted to the contact are given in Fig. 12 for zero temperature and in Fig. 13 for a finite temperature.

## III. SGM OF A DOUBLE-DOT SETUP

Instead of using a magnetic field for breaking the spin degeneracy of a single resonance, let us now show that a contact characterized by a double-peak structure of its

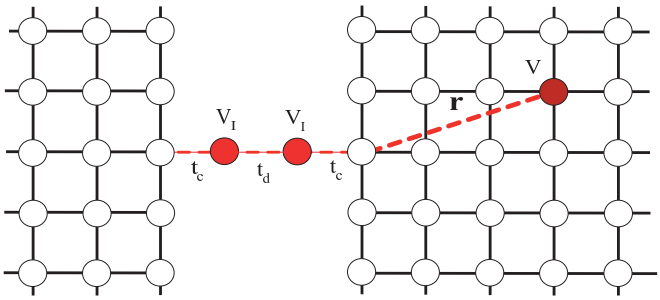


FIG. 14: (Color online) Scheme of the SGM of a contact made of two coupled identical quantum dots.

transmission without magnetic field gives rise also to a similar pattern of interference rings when it is opened between the transmission peaks. Instead of the previous single-site contact, let us consider a contact made of two sites of potentials $V_I - 4t$ coupled by an hopping term $t_d$. This gives rise to a two-level system which is often used[8] to describe electron transport through double quantum dots. A simplified lattice model relevant for describing the SGM of two well-separated identical quantum dots created in a 2DEG with a finite tunnel coupling between their levels is shown in Fig. 14. As before, the depletion region induced by the charged tip is described by a scattering site in the right lead.

Taking again $t = -1$, the Green function of this model is now given by a $2 \times 2$ matrix which reads

$$G(E) = \begin{bmatrix} E - 4 - V_I - \Sigma_l(E) & -t_d \\ -t_d & E - 4 - V_I - \Sigma_r(E) - \Delta\Sigma_r \end{bmatrix}$$

where $\Sigma_{r,l} = R + iI$ are the lead self-energies previously introduced for the RCM contact, $\Delta\Sigma_r$ being the change induced on $\Sigma_r$ by the tip. Without tip, the transmission of an electron of spin $\sigma$ reads

$$T_0^\sigma(E) = \frac{t_d}{\tilde{E}} \left( \frac{I^2}{(t_d - \tilde{E})^2 + I^2} - \frac{I^2}{(t_d - \tilde{E})^2 + I^2} \right) \quad (27)$$

where $\tilde{E} = E - 4 - V_\mathbf{I} - R$. This expression displays strong similarities with the previously studied case, where the spin degeneracy was broken by a field restricted to the contact. As before, one has two peaks of equal height and width $\Gamma/2 = -I$ (instead of $\Gamma$ for the RCM model) which are spaced by a "Zeeman energy" $2t_d$ (instead of $2h$ for the RCM model with a field restricted to the contact). Of course, the transmission of the double-dot setup is suppressed when the inter-dot coupling $t_d \to 0$, in contrast to the RCM model through which the electrons are transmitted when $h \to 0$.

These similarities are a consequence of the inversion symmetry of the double-dot model. If the two sites of the contact have respective coordinates $(0, 0)$ and $(1, 0)$, one can rewrite the Hamiltonian of the double-dot setup in terms of fermion operators which destroy/create an electron of spin $\sigma$ in an even/odd combination of two symmetric orbitals of the original model. For instance,

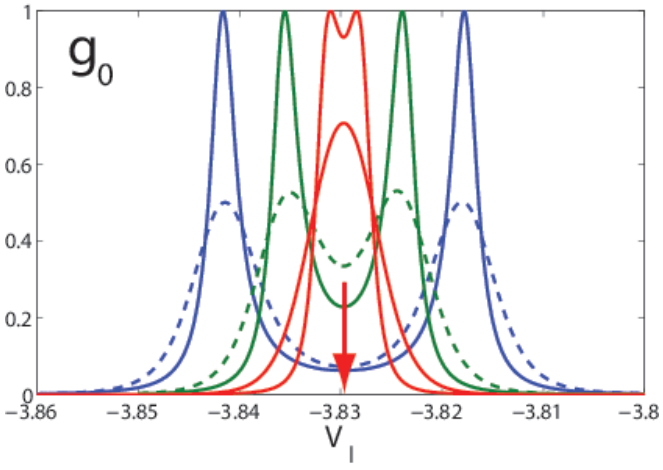


FIG. 15: (Color online) Double-dot setup without tip ($V = 0$): Conductance $g_0$ (in units of $2e^2/h$) with $t_c = 0.2$ and $\Gamma = 0.0015$ as a function of the dot potentials $V_{\mathbf{I}}$ for $t_d = 0.012$ (blue) $t_d = 0.006$ (green) and $t_d = 0.002$ (red). Cases with $\mathcal{T} = 0$ (solid line) and $\mathcal{T} = \Gamma/2$ (dashed line). The arrow gives the potential $V_{\mathbf{I}}$ used hereafter for the SGM study.

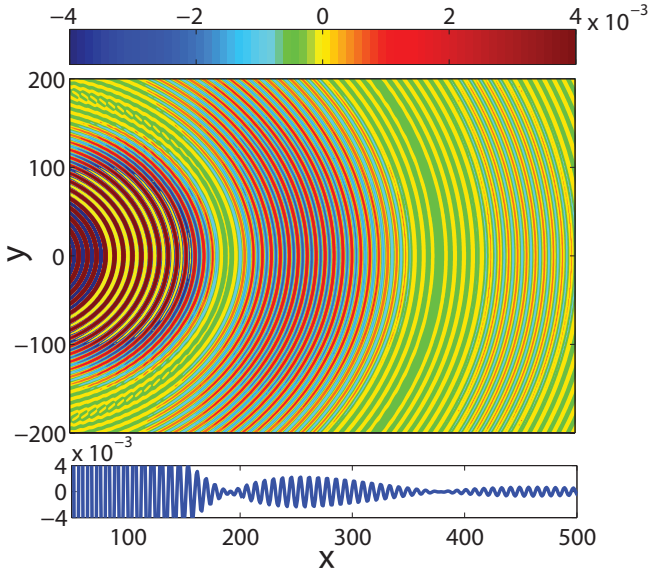


FIG. 16: (Color online) Double-dot setup - Main Fig: $\Delta g/g_0$ as a function of the tip coordinates $(x, y)$ at a temperature $\mathcal{T}^* = 0.0022$ ($g_0 = 0.3064$, $\Gamma = 0.0015$, $V = -2$, $t_d = 0.006$, $t_c = 0.2$, $E_F = 0.1542$ and $\lambda_F/2 = 8$). Above: Color code giving the magnitude of the relative effect. Below: $\Delta g/g_0(y = 0)$ as a function of $x$ (same parameters as in the main figure).

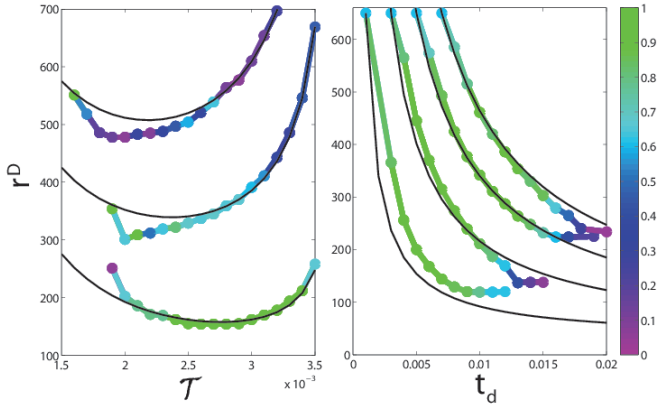


FIG. 17: (Color online) Double-dot setup with $\Gamma = 0.003$: Radii $r^{\mathcal{D}}(n)$ of the interference rings for $n = 0, 1, 2$ and 3 as a function of $\mathcal{T}$ (left fig. $t_d = 0.01$) and of the interdot coupling $t_d$ (right fig. $\mathcal{T} = 0.0028$). The dots are obtained numerically, their colors corresponding to a visibility scale indicated at the right. The solid lines are the analytical values of $r^{\mathcal{D}}(n)$ derived assuming $r^{\mathcal{D}}(n) > r^*$. This gives the ranges of temperature and interdot coupling where $r^{\mathcal{D}}(n = 0)$ is sufficiently small for seeing the rings in the SGM images.

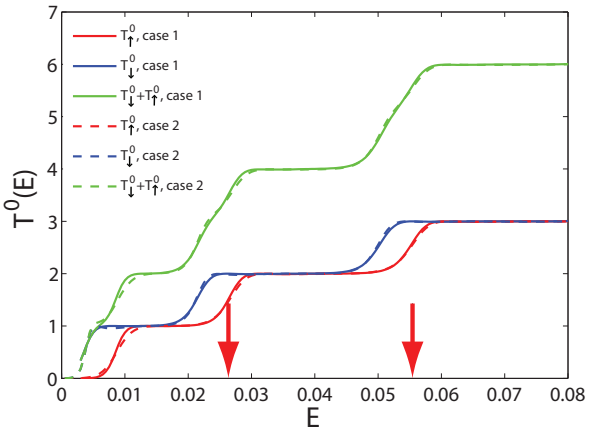


FIG. 18: (Color online) Lattice model (see Fig. 2) of a QPC without tip ($V = 0$) with $L_y = 20$, $L_x = 16$ and $k = 2$: Transmission $T^0_\sigma$ of an electron of spin $\sigma$ and total transmission $T^0 = \sum_\sigma T^0_\sigma$ as a function of $E$ when a parallel magnetic field $h = 0.0025$ is applied (case 1) everywhere and (case 2) only in the contact region ($-L_x \leq x \leq L_x$). The two arrows give the energies where the SGM images are studied.

for the destruction operators of a particle with spin $\sigma$ and pseudo-spin $e, o$, one has

$$a^{\sigma,o}_{(x,y)} = (c^\sigma_{(-x+1,-y)} - c^\sigma_{(x,y)})/\sqrt{2} \quad (28)$$

$$a^{\sigma,e}_{(x,y)} = (c^\sigma_{(-x+1,-y)} + c^\sigma_{(x,y)})/\sqrt{2}. \quad (29)$$

This allows us to map the original model (electrons with spins free to move on two semi-infinite square lattices coupled by two sites of potential $V_I$) onto a transformed model of electrons with spins and pseudo-spins (even or odd states) free to move on a single semi-infinite square lattice coupled by a single hopping term $t_c$ to a single site of potential $V_I \pm t_d$ ($+t_d$ for the odd states, $-t_d$ for the even states). In that sense, $t_d$ gives rise indeed to a "pseudo Zeeman energy" which removes the pseudo-spin degeneracy, as before $h$ was a Zeeman energy which removed the spin degeneracy. For more details about this mapping, we refer the reader to Ref.[24], where an

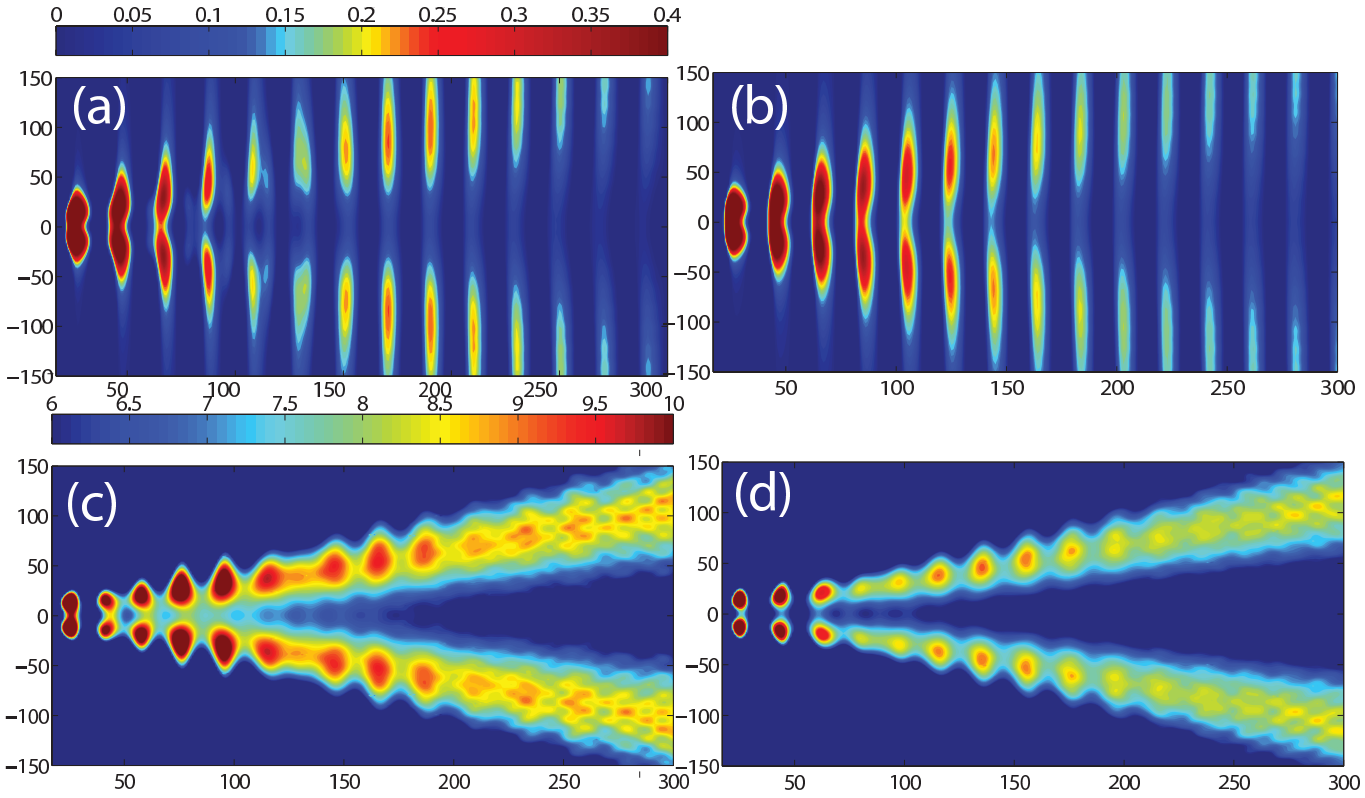


FIG. 19: (Color online). SGM images of a QPC at the opening of the second transmission channel ($E_F = 0.027$, left arrow of Fig. 18) at $\mathcal{T} = 0$ (top) and $\mathcal{T} = 0.006$ (bottom). A parallel magnetic field $h = 0.0025$ is applied everywhere (left) or only in the contact region (right). For a better visibility, we have plotted as a function of the tip coordinates $x, y$, $\frac{\delta(\Delta g)}{\delta x} \times r$ when $\mathcal{T} = 0$ and $\frac{\delta(\Delta g)}{\delta x} \times r^2$ when $\mathcal{T} = 0.006$.

inversion symmetric one dimensional model was studied, the extension to two dimensions being straightforward.

The similarity between the two models is also evident when one compares the conductance $g_0$ (in units of $2e^2/h$) of the double-dot setup shown in Fig. 15 for different values of $t_d$ and $\mathcal{T}$ with the conductance $g_0$ (in units of $e^2/h$) of the RCM model shown in Fig. 8 for different values of $h$ and $\mathcal{T}$. Such a similarity implies that their SGM images must be also similar: When $t_d \neq 0$, the SGM images of the double-dot setup should also exhibit rings where the effect of the tip does not change the conductance of the contact, the radii of these rings being given by Eq. (26), after making the changes $h \to t_d$ and $\Gamma \to \Gamma/2$. This replacement implies also that the ring spacing is equal to $\pi k_F/t_d$ for the double-dot setup. A numerical check of such a prediction is given in Fig. 16 (which shows that the SGM of the double-dot setup gives rise to a similar pattern of rings) and in Fig. 17 (which shows that the location of the rings is indeed given by Eq. (26) when one puts $t_d$ instead of $h$ and $\Gamma/2$ instead of $\Gamma$).

## IV. SGM OF A QPC WITH QUANTIZED CONDUCTANCE PLATEAUS

We now consider contacts having many sites in the transverse direction. This allows them to have more than one open transmission channel. The energy dependence of their transmission is given by a staircase function, in contrast to the single Breit-Wigner resonance of the RCM model without field. Such staircase functions with quantized conductance plateaus are observed in the setups sketched in fig. 1 where the gate potentials give rise to a smooth saddle-point QPC potential for the 2DEG. These staircase functions characterize also the lattice model for a QPC sketched in fig. 2, as it is shown in Fig. 18 in the cases where a parallel magnetic field is applied either everywhere, or only inside the contact region.

An analytical approach being more difficult, we numerically study these bigger contacts with leads made of semi-infinite square lattices of finite but very large transverse width $2\mathcal{L}_y + 1$. The self-energies $\Sigma_{l,r}(E)$ which allow us to describe them are now two matrices of size $(2L_y + 1) \times (2L_y + 1)$, where $L_y$ defines the width of the contact region (see fig. 2). Their analytical expressions without tip can be found in Ref.[20]. To include the effect of the tip which modifies the potential of a single site

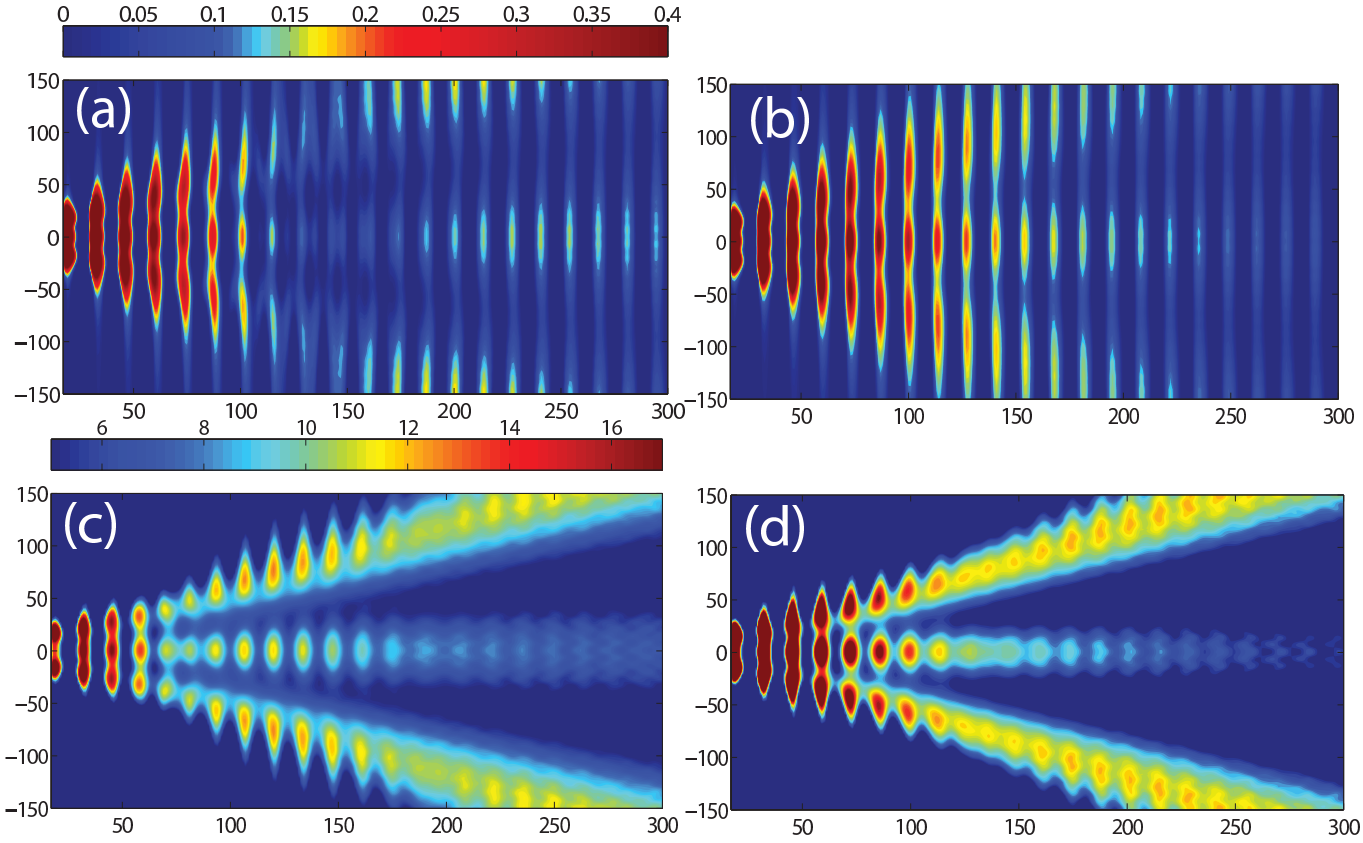


FIG. 20: (Color online). Same as Fig. 19 at the opening of the third transmission channel ($E_F = 0.056$, right arrow of Fig. 18).

in the right lead, we use again Dyson equation ($V$ playing the role of a perturbation), extending the method used for the RCM model. The usual recursive numerical method for calculating the Green function is only used for narrower contact region of smaller transverse size $\leq 2L_y + 1$. With this method, we study leads of very large transverse width $\mathcal{L}_y \approx 2.10^4$ and a contact region of size $L_x = 16$ and $L_y = 20$ where the potential $V_{\mathbf{i}}$ of a contact site $\mathbf{i}$ of coordinates $(i_x, i_y)$ is taken infinite if $|i_y| \geq (L_y - 2) + 2\,(i_x/L_x)^2)$. Once the self energies of leads with $\mathcal{N}$ open channels at an energy $E$ are obtained, the the total interferometer transmission $T(E)$ is calculated.

The channel openings of these QPCs play the role of the resonances of the RCM contact. As one can split by a parallel magnetic field the RCM resonance, one can also use it to split the QPC channel openings. The role of a parallel magnetic field upon the QPC transmission is shown in Fig. 18, both when it is applied everywhere or restricted to the contact region. For a QPC opened in the energy interval where a new channel is opened for the electrons with parallel spin, but not yet for those with antiparallel spins, it is likely that the effect of the tip upon the QPC conductance exhibits a beating of the contributions of the two channels with opposite spins, as we had the beating of the contribution of the two peaks for the RCM contact. This is indeed what can be seen in Fig. 19 when the contact is opened around the opening of the second channel, the effect of the tip having the V-shape which characterizes the second channel, or in Fig. 20 near the opening of the third channel. In each case, the QPC is opened between the openings of a new channel for the electrons with parallel and anti-parallel spins. To make the SGM images clearer, we have plotted as in Ref.[18] the effect of the tip over the conductance derivatives with respect to $x$. In panels (a) and (b) of Figs. 19 and 20, the SGM images are taken at zero temperature. One can see the beating effect between the contributions of the two channels of opposite spins when the field is applied everywhere, but not when the field is restricted to the contact region. In panels (c) and (d), the SGM images are taken at a temperature $\mathcal{T} = 0.006$, and one can see also the beating effect when the field is applied only in the contact region. Similar behaviors were observed and explained previously using the RCM contact.

## V. CONCLUSION

In summary, we have studied contacts where the transmission exhibits a resonance or a channel opening. When the spin degeneracy is broken by a magnetic field $h$ or the pseudo-spin degeneracy by an inter-dot coupling $t_d$, one can split the resonance or the channel opening. We have

shown that imaging these contacts opened between the split resonances or channel openings with a scanning gate microscope gives rings where the effect of the tip is totally suppressed. If the magnetic field is applied everywhere, these rings are produced by a beating effect between the contributions of opposite spins which can be observed at zero temperature. If the field is applied upon the contact only, the temperature has to be around an optimum temperature $\mathcal{T}^*$ of order of the peak spliting, such that the first rings are sufficiently close to the contact for being observable. When $\mathcal{T} \to 0$, the radii of the rings $r^{\mathcal{D}} \to \infty$ and the beating effect disappears.

The spacing of the Fabry-Pérot fringes being $\lambda_F/2$, we underline that SGM provides a new method for measuring by electron interferometry $\lambda_F$ together with either the magnetic field $h$ (RCM-contact) or the inter-dot coupling $t_d$ (double-dot setup). The spacing between the rings is $\pi k_F/h$ in the first case or $\pi k_F/t_d$ in the second case.

We have studied the ring pattern at the symmetric point between the resonances or the channel openings. If one opens the contact in the vicinity of the symmetric point, the effect of the tip remains modulated without canceling exactly on rings, as one scans the tip around the contact. Similarly, if one takes the double-dot setup with different terms $t_c$ for the right and left couplings, the inversion symmetry is removed and one gets two transmission peaks of different widths. Nevertheless, one can still observe a beating phenomenon when the contact transmission varies between the peaks. We conclude that beating phenomena between contributions of different spins or pseudo-spins are generic phenomena, while rings with exact cancellation require a symmetry, as a spin or a pseudo-spin rotation symmetry. With such a symmetry, one gets two split resonances of identical width, and the effect of the tip is totally suppresed on rings at the symmetric point.

We have shown that these beating effects can also be seen in the SGM images of a QPC with quantized conductance plateaus, in the vicinity of a spin-split channel opening. As for the RCM model, we have underlined the difference between a local or a global Zeeman effect. This leads us to conclude that these beating effects are generic interference phenomena.

### Acknowledgments

This research has been supported by the EU Marie Curie network "NanoCTM" (project no.234970). Discussions with B. Brun, K. Ensslin, M. Sanquer and H. Sellier about SGM experiments and with C. Gorini, R. Jalabert and D. Weinmann about SGM theory are gratefully acknowledged.

[1] M. Topinka, R. Westervelt, and E. Heller, Physics Today **56**, 47 (2003).
[2] B. J. van Wees, H. van Houten, C. W. J. Beenakker, J. G. Williamson, L. P. Kouwenhoven, D. van der Marel, and C. T. Foxon, Phys. Rev. Lett. **60**, 848 (1988).
[3] K. J. Thomas, J. T. Nicholls, M. Y. Simmons, M. Pepper, D. R. Mace, and D. A. Ritchie, Phys. Rev. Lett. **77**, 135 (1996).
[4] D. Goldhaber-Gordon, H. Shtrikman, D. Mahalu, D. Abusch-Magder, U. Meirav, and M. A. Kastner, Nature **391**, 156 (1998).
[5] S. Cronenwett, T. H. Oosterkamp, and L. P. Kouwenhoven, Science **281**, 540 (1998).
[6] M. Grobis, I. G. Rau, R. M. Potok, and D. Goldhaber-Gordon, in *Handbook of Magnetism and Magnetic Materials*, edited by H. Kronmuller and S. Parkin (Wiley, 2007).
[7] N. C. van der Vaart, S. F. Godijn, Y. V. Nazarov, C. J. P. M. Harmans, J. E. Mooij, L. W. Molenkamp, and C. T. Foxon, Phys. Rev. Lett. **74**, 4702 (1995).
[8] W. G. van der Wiel, S. De Francheschi, J. M. Elzerman, T. Fujisawa, S. Tarucha, and L. P. Kouwenhoven, Rev. Mod. Phys. **75**, 1 (2002).
[9] M. Topinka, B. LeRoy, S. Shaw, E. Heller, R. Westervelt, K. Maranowski, and A. Gossard, Science **289**, 2323 (2000).
[10] E. Heller, K. Aidala, B. LeRoy, A. Bleszynski, A. Kalben, R. Westervelt, K. Maranowski, and A. Gossard, Nano Lett. **5**, 1285 (2005).
[11] G. Metalidis and P. Bruno, Phys. Rev. B **72**, 235304 (2005).
[12] A. Freyn, I. Kleftogiannis, and J.-L. Pichard, Phys. Rev. Lett. **100**, 226802 (2008).
[13] R. A. Jalabert, W. Szewc, S. Tomsovic, and D. Weinmann, Phys. Rev. Lett. **105**, 166802 (2010).
[14] A. Abbout, G. Lemarié, and J.-L. Pichard, Phys. Rev. Lett. **106**, 156810 (2011).
[15] C. Gorini, R. A. Jalabert, W. Szewc, S. Tomsovic, and D. Weinmann, Phys.Rev.B **88**, 035406 (2013).
[16] C. Gorini, D. Weinmann, and R. A. Jalabert, Phys.Rev.B **89**, 115414 (2014).
[17] M. P. Nowak, K. Kolasinski, and B. Szafran, Phys.Rev.B **90**, 035301 (2014).
[18] A. A. Kozikov, C. Rossler, T. Ihn, K. Ensslin, C. Reichl, and W. Wegscheider, New Journal of Physics **15**, 013056 (2013).
[19] B. Brun, F. Martins, S. Faniel, B. Hackens, G. Bachelier, A. Cavanna, C. Ulysse, A. Ouerghi, U. Gennser, D. Mailly, et al., Nature Communications **5** (2014).
[20] S. Datta, *Electronic transport in mesoscopic systems* (Cambridge Univ Pr, 1997).
[21] M. I. Molina, Phys. Rev. B **74**, 045412 (2006).
[22] E. Economou, *Green's functions in quantum physics* (Springer Verlag, 2006).
[23] P. Darancet, V. Olevano, and D. Mayou, Phys. Rev. B **81**, 155422 (2010).
[24] A. Freyn and J.-L. Pichard, Phys. Rev. B **81**, 085108 (2010).